TU Delft

Delft University of Technology

Segmentation-assisted vessel centerline extraction from cerebral CT Angiography

Liu, Sijie; Su, Ruisheng; Su, Jianghang; van Zwam, Wim H.; van Doormaal, Pieter Jan; van der Lugt, Aad; Niessen, Wiro J.; van Walsum, Theo

DOI
10.1002/mp.17855

Publication date
2025

Document Version
Final published version

Published in
Medical Physics

Citation (APA)
Liu, S., Su, R., Su, J., van Zwam, W. H., van Doormaal, P. J., van der Lugt, A., Niessen, W. J., & van Walsum, T. (2025). Segmentation-assisted vessel centerline extraction from cerebral CT Angiography. *Medical Physics*, *52*(7), Article e17855. https://doi.org/10.1002/mp.17855

Important note
To cite this publication, please use the final published version (if applicable).
Please check the document version above.

Copyright
Other than for strictly personal use, it is not permitted to download, forward or distribute the text or part of it, without the consent of the author(s) and/or copyright holder(s), unless the work is under an open content license such as Creative Commons.

Takedown policy
Please contact us and provide details if you believe this document breaches copyrights.
We will remove access to the work immediately and investigate your claim.

This work is downloaded from Delft University of Technology.
For technical reasons the number of authors shown on this cover page is limited to a maximum of 10.

Check for updates

Received: 13 May 2024 | Revised: 7 March 2025 | Accepted: 8 April 2025

DOI: 10.1002/mp.17855

RESEARCH ARTICLE

MEDICAL PHYSICS

Segmentation-assisted vessel centerline extraction from cerebral CT Angiography

Sijie Liu[1,2,3] | **Ruisheng Su**[2,4] | **Jiahang Su**[2] | **Wim H. van Zwam**[5] | **Pieter Jan van Doormaal**[2] | **Aad van der Lugt**[2] | **Wiro J. Niessen**[2,6] | **Theo van Walsum**[2]

[1]Institute of Applied Electronics, China Academy of Engineering Physics, Mianyang, China

[2]Department of Radiology & Nuclear Medicine, Erasmus MC, University Medical Center Rotterdam, Rotterdam, The Netherlands

[3]National Key Laboratory of Science and Technology on Advanced Laser and High Power Microwave, China Academy of Engineering Physics, Mianyang, China

[4]Medical Image Analysis Group, Department of Biomedical Engineering, Eindhoven University of Technology, Eindhoven, The Netherlands

[5]Department of Radiology & Nuclear Medicine, Maastricht UMC, Cardiovascular Research Institute Maastricht, Maastricht, The Netherlands

[6]Imaging Physics, Department of Applied Sciences, Delft University of Technology, Delft, The Netherlands

Correspondence
Ruisheng Su, Department of Radiology and Nuclear Medicine, Erasmus MC, University Medical Center Rotterdam, Rotterdam, The Netherlands.
Email: r.su@tue.nl

Sijie Liu and Ruisheng Su contributed equally to this work.

Funding information
Health Holland, Grant/Award Number: EMCLSH19006; National Key Research and Development Program of China, Grant/Award Number: 2017YFA0700800; Philips Healthcare

[Correction added on 12 June 2025, after first online publication: The third author's name was updated from Jianghang Su to Jiahang Su.]

Abstract

Background: The accurate automated extraction of brain vessel centerlines from Computed tomographic angiography (CTA) images plays an important role in diagnosing and treating cerebrovascular diseases such as stroke. Despite its significance, this task is complicated by the complex cerebrovascular structure and heterogeneous imaging quality.

Purpose: This study aims to develop and validate a segmentation-assisted framework designed to improve the accuracy and efficiency of brain vessel centerline extraction from CTA images. We streamline the process of lumen segmentation generation without additional annotation effort from physicians, enhancing the effectiveness of centerline extraction.

Methods: The framework integrates four modules: (1) pre-processing techniques that register CTA images with a CT atlas and divide these images into input patches, (2) lumen segmentation generation from annotated vessel centerlines using graph cuts and robust kernel regression, (3) a dual-branch topology-aware UNet (DTUNet) that optimizes the use of the annotated vessel centerlines and the generated lumen segmentation via a topology-aware loss (TAL) and its dual-branch structure, and (4) post-processing methods that skeletonize and refine the lumen segmentation predicted by the DTUNet.

Results: An in-house dataset derived from a subset of the MR CLEAN Registry is used to evaluate the proposed framework. The dataset comprises 10 intracranial CTA images, and 40 cube CTA sub-images with a resolution of $128 \times 128 \times 128$ voxels. Via five-fold cross-validation on this dataset, we demonstrate that the proposed framework consistently outperforms state-of-the-art methods in terms of average symmetric centerline distance (ASCD) and overlap (OV). Specifically, it achieves an ASCD of 0.84, an $OV_{1.0}$ of 0.839, and an $OV_{1.5}$ of 0.885 for intracranial CTA images, and obtains an ASCD of 1.26, an $OV_{1.0}$ of 0.779, and an $OV_{1.5}$ of 0.824 for cube CTA sub-images. Subgroup analyses further suggest that the proposed framework holds promise in clinical applications for stroke diagnosis and treatment.

Conclusions: By automating the process of lumen segmentation generation and optimizing the network design of vessel centerline extraction, DTUnet achieves high performance without introducing additional annotation demands.

This is an open access article under the terms of the Creative Commons Attribution-NonCommercial License, which permits use, distribution and reproduction in any medium, provided the original work is properly cited and is not used for commercial purposes.
© 2025 The Author(s). *Medical Physics* published by Wiley Periodicals LLC on behalf of American Association of Physicists in Medicine.

This solution promises to be beneficial in various clinical applications in cerebrovascular disease management.

KEYWORDS
brain, cerebrovascular disorders, deep learning, stroke, x-ray computed tomography

1 | INTRODUCTION

Stroke is globally the second leading cause of death and the third leading cause of disability, affecting approximately 15 million people each year.[1] As an acute cerebrovascular disease, stroke is characterized by significant changes in brain vessels, such as rupture or occlusion. Therefore, understanding the cerebrovascular structure is relevant in clinical settings for the prevention, assessment, prognosis, and treatment of stroke.[2] Computed tomographic angiography (CTA) is a minimally invasive imaging technique that effectively visualizes intracranial vessels and is widely used in the diagnosis and treatment decision-making for stroke patients. Automated cerebrovascular analysis, including the detection of vessels and related diseases, could provide valuable support to clinicians and interventionists.[3,4] For example, cerebrovascular structure extraction is beneficial for localizing vessel occlusions[5] and calculating collateral scores.[6] In clinical practice, accurately detecting cerebrovascular occlusions is crucial for physicians to determine the type and severity of cerebral infarction, thereby guiding the selection of appropriate treatment strategies. Assessing the status of collateral circulation provides insight into the potential for salvageable brain tissue, which can significantly influence the clinical outcomes of patients undergoing endovascular therapy. Furthermore, automated centerline extraction is instrumental in aiding vessel segmentation[7] and facilitating brain registration.[8] However, accurate automated extraction of brain vessel centerlines from CTA images remains challenging due to the complex nature of cerebrovascular structures and heterogeneous imaging quality.

Traditional approaches for vessel centerline extraction can be broadly divided into three categories: morphology-based, distance transformation-based, and model evolution-based methods. Morphology-based methods skeletonize pre-segmented 3D vessels to derive centerlines. Palágyi et al.[9] introduced an 8-direction thinning rule to extract vessel topologies. Cheng et al.[10] developed a robust thinning algorithm that incorporates line direction filters across 13 orientations to enhance small vessels. Distance transformation-based methods involve extracting centerlines from a distance map where each voxel value represents its minimum distance to the nearest vascular edge. He et al.[11] employed a reliable path approach to identify central paths, which were subsequently converted to vessel centerlines. Similarly, Jin et al.[12] proposed a curve skeletonization algorithm based on a minimum cost path strategy. Model evolution-based methods start with initial centerline extraction using axis detection, and subsequently refine these centerlines by minimizing an energy function. Krissian et al.[13] developed a multiscale centerline detection algorithm based on a cylindrical model, which also estimates the radius of the vessels simultaneously. Fung et al.[14] modeled vessel centerlines using cubic B-spline curves, which consist of 3D cubic polynomial segments. However, due to the diversity and complexity of medical images, these traditional approaches that rely on hand-designed features struggle to generalize effectively to new and unseen datasets, leading to limited accuracy in practical applications.

Recent advancements in deep learning have shown promising results in vessel segmentation, primarily due to their robust feature representation capabilities.[15,16] Therefore, some studies have leveraged lumen segmentation results to extract vessel centerlines. Guo et al.[17] employed a multi-task convolutional network to produce centerline distance maps and endpoint maps from segmentation masks of coronary CTA images, subsequently applying a minimal cost path algorithm to derive the centerlines. Similarly, Tetteh et al.[18] introduced DeepVesselNet, capable of handling multiple vessel-related tasks, including vessel segmentation, centerline extraction, and bifurcation detection. DeepVesselNet employs the output of the vessel segmentation to train the centerline extraction model. He et al.[19] also leveraged vessel segmentation to guide centerline heatmap regression, followed by a minimal cost path to obtain the final vessel centerline. Despite these innovations, such methods rely heavily on the additional annotation from lumen segmentation, complicating the centerline extraction process. Given the significant variations in the shape, size, and intensity of the brain's luminal structures, accurately delineating the lumen border of extensive cerebral vessels could be challenging and labor-intensive. Furthermore, the requirement for extensive training data in current deep-learning approaches places an additional burden on experienced annotators, highlighting a bottleneck in the scalability of such methods.

Recent efforts have also investigated methods that rely only on the annotation of vessel centerlines. Sironi et al.[20] proposed a multi-scale centerline regressor to predict distance maps from annotated centerlines, employing a non-maximum suppression algorithm to extract the centerlines from these maps. Rjiba et al.[21]

24734209, 2025, 7, Downloaded from https://aapm.onlinelibrary.wiley.com/doi/10.1002/mp.17855, Wiley Online Library on [21/07/2025]. See the Terms and Conditions (https://onlinelibrary.wiley.com/terms-and-conditions) on Wiley Online Library for rules of use; OA articles are governed by the applicable Creative Commons License

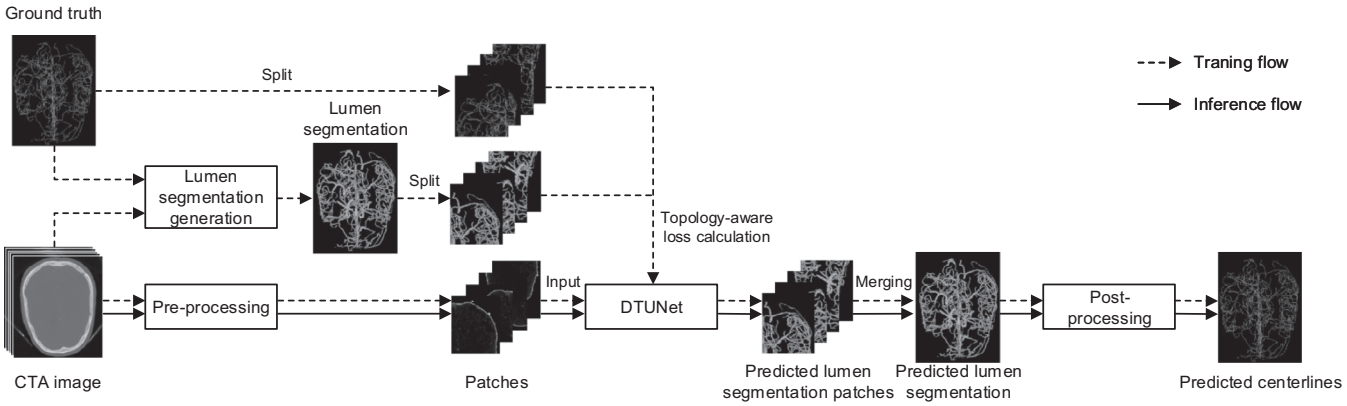

FIGURE 1 Overview of the proposed framework illustrating the training and inference phases. The training phase, depicted with dashed lines, consists of four modules, pre-processing, lumen segmentation generation, DTUNet, and post-processing. The inference phase, shown with solid lines, does not require the lumen segmentation generation. DTUNet, dual-branch topology-aware UNet.

introduced CenterlineNet, which extracts the main and side branches of coronary artery centerlines. Su et al.[6] utilized a 3D UNet to directly extract dilated vessel centerlines from brain CTA images. Although these studies have shown promising results, they generally do not consider the topological connections among different vessel segments. Addressing this gap, Zhang et al.[22] designed a C-UNet that initially extracts preliminary vessel centerlines from coronary angiography images and subsequently applies a multi-factor centerline reconnection algorithm to enhance the continuity of these centerlines. And some studies[23,24] investigated tracking-based approaches to extract connected vessel centerlines. While these approaches are well-suited for simple scenarios with a limited number of vessel centerlines, they may face challenges in cerebral vascular imaging where hundreds of vessel centerlines are present.

In this study, we explore the automatic lumen segmentation generation without additional annotation effort by physicians and subsequently leverage these segmentations to improve centerline extraction. To this end, we introduce a segmentation-assisted framework for brain vessel centerline extraction from CTA images, as illustrated in Figure 1. This framework not only generates lumen segmentation based on annotated vessel centerlines, but also incorporates a dual-branch topology-aware UNet (DTUNet) to effectively exploit both the annotated vessel centerlines and the generated lumen segmentation. The main contributions are as follows:

- We demonstrate that introducing the lumen segmentation generated from annotated centerlines during the training phase can improve the performance of brain vessel centerline extraction. This segmentation generation is not required during inference, thus avoiding additional computational demands.
- We introduce DTUNet which incorporates a two-branch structure and a topology-aware loss to effectively utilize the annotated vessel centerlines and the generated lumen segmentation.
- We demonstrate the superior performance and clinical potential of the proposed framework through comprehensive experiments and subgroup analyses on an in-house dataset derived from a subset of the MR CLEAN Registry.

2 | METHODS

The proposed framework for brain vessel centerline extraction from CTA images is illustrated in Figure 1. It mainly consists of four modules: (1) pre-processing, (2) lumen segmentation generation, (3) DTUNet, and (4) post-processing. The details of all the components are elaborated in the following.

2.1 | Data description and pre-processing

In this study, we used CTA images from a subset of the MR CLEAN Registry,[25] a national multi-center registry for patients who underwent endovascular treatment in the Netherlands between March 2014 and January 2019. Fifty representative CTA images from patients with acute ischemic stroke were manually annotated by experienced observers[6] using Mevislab.[26] Ten out of the 50 images are with intracranial vessel centerline annotations, hereinafter referred to as intracranial CTA images. The remaining 40 images have vessel centerline annotations for a randomly sampled sub-volume with $128 \times 128 \times 128$ voxels, hereinafter referred to as cube CTA images.

24734209, 2025, 7, Downloaded from https://aapm.onlinelibrary.wiley.com/doi/10.1002/mp.17855, Wiley Online Library on [21/07/2025]. See the Terms and Conditions (https://onlinelibrary.wiley.com/terms-and-conditions) on Wiley Online Library for rules of use; OA articles are governed by the applicable Creative Commons License

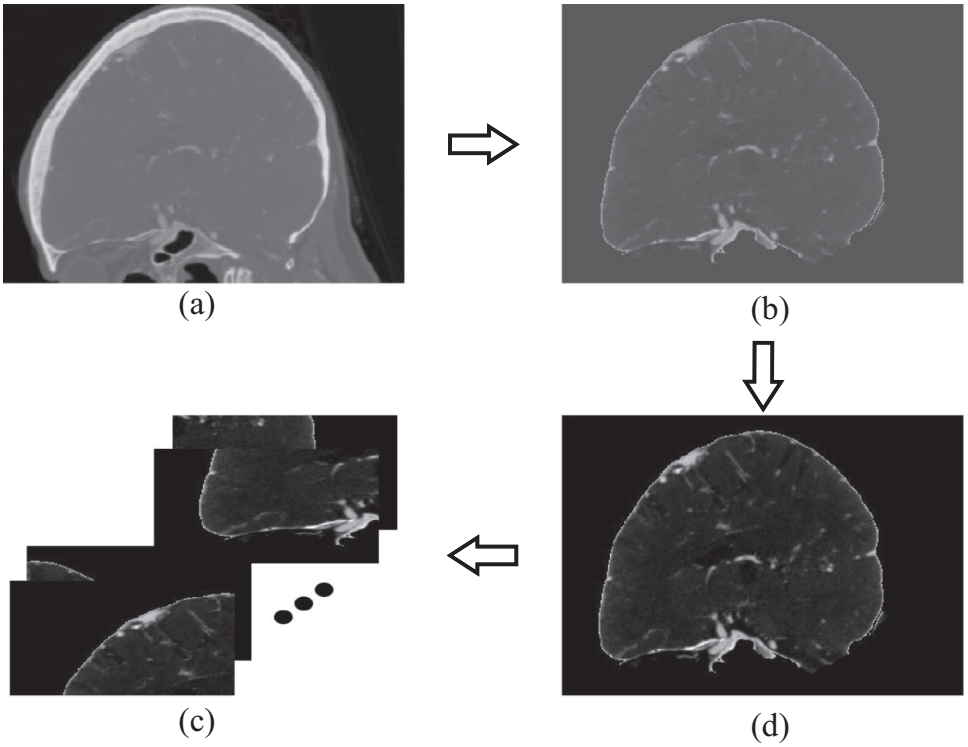

FIGURE 2 Illustration of the pre-processing procedure: (a) raw CTA image; (b) image after registration and masking; (c) clipped and normalized image; (d) split patches. CTA, Computed tomographic angiography.

The objective of pre-processing is to align CTA images with a CT atlas and to subdivide the CTA images into patches. We adopt similar pre-processing approaches outlined in ref. [6], as illustrated in Figure 2. First, we use a CT altas, which is constructed from the average of high-resolution 3D CTA images of 30 healthy subjects,[27] along with its corresponding binary brain mask. We use advanced normalization tools (ANTs)[28] to register the atlas to each CTA image, after which the corresponding registered brain mask is applied to the images to set all non-brain voxels to zero. Next, the voxel values are clipped between 0 and 850 Hounsfield Units (HU) based on the intensity distribution of annotated vessel centerlines, after which these values are normalized to a range of 0 – 1. Lastly, we split CTA images into patches. During the training phase, we split the intracranial CTA images into $64 \times 64 \times 64$ overlapping patches with a stride of 16 and removed the patches with no vessel present. From each of the CTA images, we select the 500 patches with the highest vessel centerline densities, and randomly extract 500 patches from the remaining patches. To enhance the diversity among the overlapping patches, we split the cube CTA images of size $128 \times 128 \times 128$ voxels into $64 \times 64 \times 64$ patches using a larger stride of 32. This approach increases the variety of extracted patches. We then remove any patches that do not contain vessels. In this way, we obtain 11 058 patches with $64 \times 64 \times 64$ voxels from the intracranial and cube CTA images. During the inference phase, we split all the intracranial and cube CTA images into 4416 non-overlapping patches with $64 \times 64 \times 64$ voxels. Statistics of all the CTA patches are shown in Table 1.

TABLE 1 Statistics of the CTA patches extracted from the intracranial and cube CTA images.

Phase	Intracranial	Cube	Total
Training	10 000	1058	11 058
Inference	4096	320	4416

Abbreviation: CTA, computed tomographic angiography.

2.2 | Lumen segmentation generation

The purpose of the lumen segmentation generation is to provide additional supervisory information for training deep neural networks. The process is structured into a three-step procedure, as illustrated in Figure 3. First, following the approach of Schaap et al.,[29] we resample the image along the annotated centerline[6] to obtain slices orthogonal to the centerline. Subsequently, a graph-cut method[30] is applied to create lumen segmentation in the cross-sectional slices, followed by robust kernel regression[31] to smooth the border of the lumen segmentation. Finally, the complete brain lumen segmentation is created from the cross-sectional segmentation using an interpolation approach.[32] For better understanding, the pseudo-code of the lumen segmen-

24734209, 2025, 7, Downloaded from https://aapm.onlinelibrary.wiley.com/doi/10.1002/mp.17855, Wiley Online Library on [21/07/2025]. See the Terms and Conditions (https://onlinelibrary.wiley.com/terms-and-conditions) on Wiley Online Library for rules of use; OA articles are governed by the applicable Creative Commons License

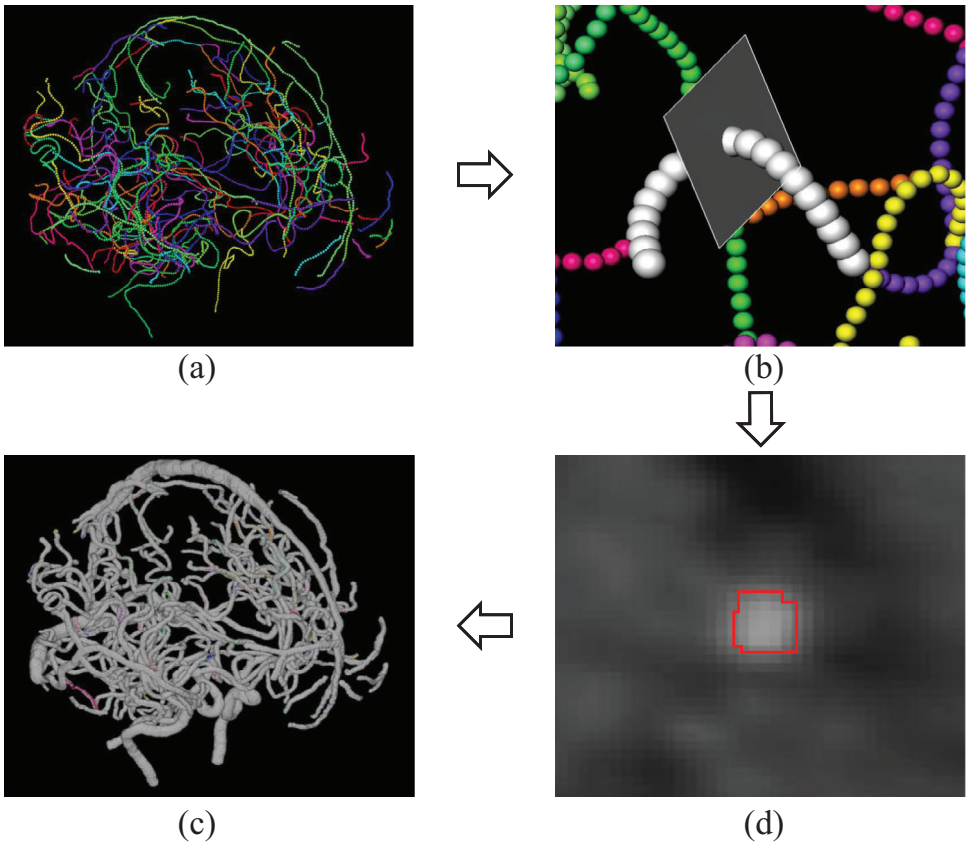

FIGURE 3 Illustration of the lumen segmentation generation procedure: (a) annotated of cerebral vessel centerlines where each centerline segment is assigned a different color; (b) a cross-sectional slice obtained along a centerline; (c) lumen segmentation obtained from a slice using graph cuts and robust kernel regression; (d) complete brain lumen segmentation created using an interpolation approach.

tation generation is presented in Algorithm 1. Like the CTA image, the annotated centerline and the generated lumen segmentation are partitioned into patches for training. Notably, the annotated centerline and the generated lumen segmentation are not required for inference.

2.3 | DTUNet

In order to effectively exploit the annotated vessel centerline and the generated lumen segmentation during the training phase, we propose a dual-branch network architecture based on 3D UNet,[33] and utilize a topology-aware loss (TAL) function that optimizes the consistency of the topological connectivity between vessel centerlines and lumen segmentation.

2.3.1 | Network architecture

The DTUNet (Figure 4) is a 3D UNet-based network with two branches and a fusion path (FP). The shared layers of the DTUNet consist of three convolutional blocks, where each block has two 3D convolutional layers followed by a max pooling layer. The first block takes a patch of $64 \times 64 \times 64$ voxels as input and has 32 initial convolutional filters to reduce GPU memory consumption. The number of convolutional filters in the subsequent blocks is chosen according to the design rule of 3D UNet.[33] The first branch is used to predict lumen segmentation and the second branch is used to predict vessel centerlines. Both branches have the same architecture, comprising one convolutional block without the max pooling layer, three deconvolutional blocks, and one 3D convolutional layer followed by a sigmoid layer. Each deconvolution block has one 3D deconvolutional layer followed by two 3D convolutional layers. The FP, which includes three fusion blocks, is positioned between the two branches to effectively enhance the information interaction between the two branches. The fusion block, as shown in Figure 5, employs a concatenation operation and a convolutional layer to aggregate features from the two branches. It then utilizes a channel attention module and a spatial attention module to automatically emphasize task-related features. These features are combined with the aggregated features at the end. Specifically, given an input feature $F \in \mathbb{R}^{H \times W \times L \times C}$, the channel attention feature M_c is

24734209, 2025, 7, Downloaded from https://aapm.onlinelibrary.wiley.com/doi/10.1002/mp.17855, Wiley Online Library on [21/07/2025]. See the Terms and Conditions (https://onlinelibrary.wiley.com/terms-and-conditions) on Wiley Online Library for rules of use; OA articles are governed by the applicable Creative Commons License

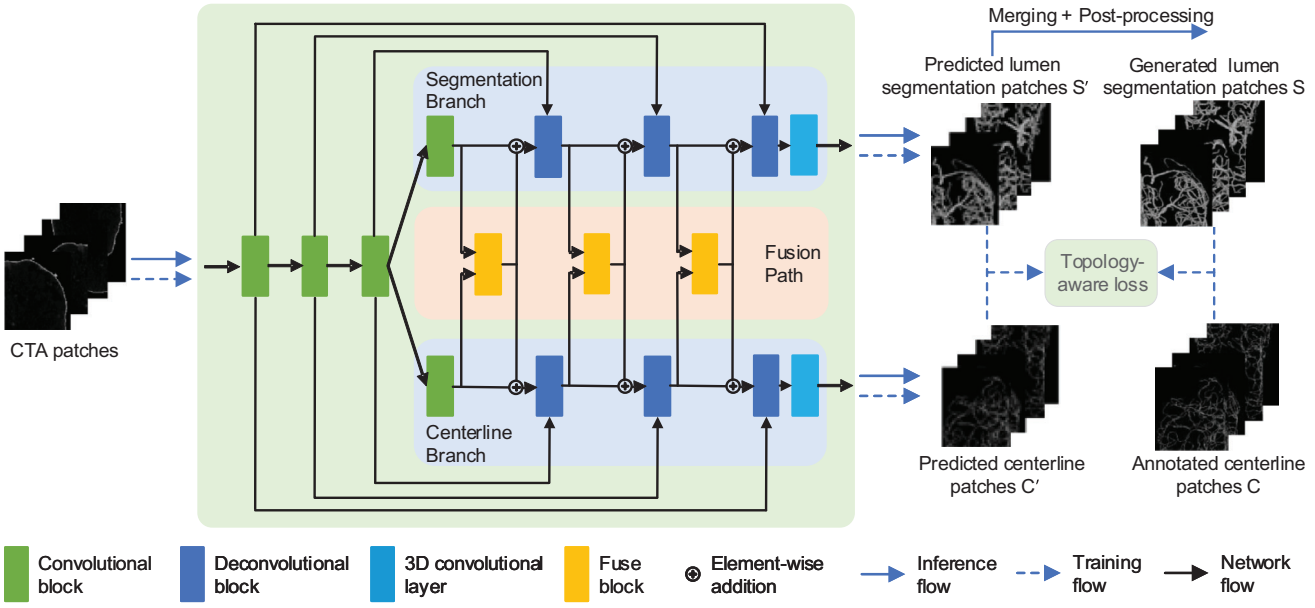

FIGURE 4 Schematic diagram of the DTUNet. The predicted lumen segmentation patches S' output are used to obtain final vessel centerlines via a merging operation and post-processing techniques. DTUNet, dual-branch topology-aware UNet.

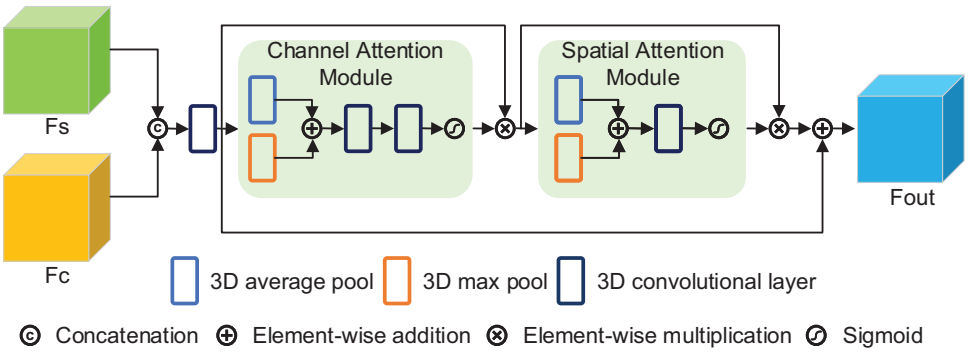

FIGURE 5 Diagram of the fusion block. This component integrates features F_s from the segmentation branch and F_c from the centerline branch.

computed as:

$$M_c = F \otimes \sigma(W_1(W_2(\text{AvgPool}_c(F) + \text{MaxPool}_c(F)))) \quad (1)$$

where $\otimes$, σ, and W denote the element-wise multiplication, the sigmoid function, and the 3D convolutional layer, respectively. Note that AvgPool_c and MaxPool_c denote the 3D-average-pool and 3D-max-pool operations that are conducted along the channel dimension. Similarly, the spatial attention feature M_s is computed as:

$$M_s = F \otimes \sigma(W_1(\text{AvgPool}_s(F) + \text{MaxPool}_s(F)) \quad (2)$$

where AvgPool_s and MaxPool_s denote the 3D-average-pool and 3D-max-pool operations that are conducted along the spatial dimension. Given a feature of the segmentation branch F_s and a feature of the centerline branch F_c, the fusion block outputs a feature $F_{out} \in \mathbb{R}^{H\times W\times L\times C}$ that is formulated as:

$$F_{out} = \text{A}(F_s, F_c) \otimes (1 + M_s(M_c(\text{A}(F_s, F_c))) \quad (3)$$

where A denotes the combination of the concatenation operation and the 3D convolutional layer.

2.3.2 | Loss function

A TAL function is designed to optimize the DTUNet by fully leveraging the generated lumen segmentation and the annotated vessel centerlines. This TAL consists of three terms: the Dice loss for the lumen segmentation, the Dice loss for the vessel centerline and the centerline Dice (clDice) loss.[34] Specifically, the Dice loss for the lumen segmentation is intended for the optimization of the overlap between the predicted lumen segmentation

24734209, 2025, 7, Downloaded from https://aapm.onlinelibrary.wiley.com/doi/10.1002/mp.17855, Wiley Online Library on [21/07/2025]. See the Terms and Conditions (https://onlinelibrary.wiley.com/terms-and-conditions) on Wiley Online Library for rules of use; OA articles are governed by the applicable Creative Commons License

ALGORITHM 1 Lumen segmentation generation.

Input: Annotated vessel centerlines V
Output: Brain lumen segmentation L
$k \leftarrow$ obtain the number of centerline segments in V;
for $i \leftarrow 1$ **to** k **do**
  $n \leftarrow$ obtain the number of centerline points in the centerline segment V_i;
  for $j \leftarrow 1$ **to** n **do**
    $C_i^j \leftarrow$ obtain the cross sectional slice of the vessel centerline point V_i^j;
    $S_i^j \leftarrow$ predict the lumen segmentation in C_i^j using the graph-cut method;
  end
  $S_i \leftarrow$ smooth the border of S_i using the robust kernel regression;
end
return $L \leftarrow$ create the complete brain lumen segmentation from all the lumen segmentation S using the interpolation approach;

and the lumen segmentation generated by the lumen segmentation generation algorithm, and is defined as:

$$L_{Dice}^{seg} = 1 - 2\frac{|S \cap S'|}{|S| + |S'|} \tag{4}$$

where S is the lumen segmentation generated by the lumen segmentation generation algorithm, and S' is the corresponding predicted result. The Dice loss for the vessel centerline is intended for the optimization of the overlap between the predicted vessel centerline and the annotated vessel centerline, and is defined as:

$$L_{Dice}^{cen} = 1 - 2\frac{|C \cap C'|}{|C| + |C'|} \tag{5}$$

where C is the annotated vessel centerline, and C' is the corresponding predicted result. The clDice loss is intended for the optimization of the consistency of the topological connectivity between the predicted vessel centerline and the predicted lumen segmentation, and is defined as:

$$L_{clDice} = 1 - 2\frac{\text{Tprec}(S, C') \times \text{Tsens}(S', C)}{\text{Tprec}(S, C') + \text{Tsens}(S', C)} \tag{6}$$

where $\text{Tprec}(S, C')$ and $\text{Tsens}(S', C)$ are calculated as:

$$\text{Tprec}(S, C') = \frac{|S \cap C'|}{C'} \tag{7}$$

$$\text{Tsens}(S', C) = \frac{|S' \cap C|}{C} \tag{8}$$

where $\text{Tprec}(S, C')$ ensures that the predicted vessel centerline is within the generated lumen segmentation as much as possible, while $\text{Tsens}(S', C)$ ensures that the annotated vessel centerline is within the predicted lumen segmentation. Maximizing both the $\text{Tprec}(S, C')$ and $\text{Tsens}(S', C)$ results in an optimal value for the L_{clDice}, and causes the predicted vessel centerline to lie within the predicted lumen segmentation.

The L_{clDice} differs with soft-clDice[34] in the computation process, as illustrated in Figure 6. The soft-clDice obtains the predicted vessel centerline from the predicted lumen segmentation by using a soft-skeleton algorithm. In contrast, the L_{clDice} directly derives the predicted vessel centerline from the centerline branch. This implies that L_{clDice} could strengthen information interaction between the two branches.

Finally, these three loss functions are combined as follows:

$$\text{TAL} = (1 - \alpha) \cdot (0.5 \cdot L_{Dice}^{seg} + 0.5 \cdot L_{Dice}^{cen}) + \alpha \cdot L_{clDice} \tag{9}$$

where α is a hyper-parameter that balances the loss components.

2.4 | Post-processing

To derive the final vessel centerlines from the lumen segmentation produced by the segmentation branch, post-processing is required. While the soft-clDice method[34] initially improved lumen segmentation quality, its soft-skeleton algorithm is designed for gradient backpropagation purposes rather than for smoothing the vessel centerlines. This often results in the generation of numerous small, isolated centerline segments composed of only a few adjacent points. To address this, we employ a medial surface/axis thinning algorithm[35] instead of the soft-skeleton algorithm to extract the final vessel centerline from the lumen segmentation output by the segmentation branch. This approach produces superior results compared to those directly output by the center branch, as detailed in Section 3.6.

3 | EXPERIMENTS AND RESULTS

3.1 | Implement details

We implemented the lumen segmentation generation in MevisLab. We implemented the pre-processing, the DTUNet, and the post-processing in Python and Pytorch.[36] We trained the DTUNet on an Nvidia GTX 2080 TI with a batch size of 4. We applied data augmentation techniques including random flip and random elastic deformation. We used the Adam[37] optimizer with an initial learning rate of 10^{-3} and a weight decay of 5×10^{-4}. We adopted a five-fold cross-validation

24734209, 2025, 7, Downloaded from https://aapm.onlinelibrary.wiley.com/doi/10.1002/mp.17855, Wiley Online Library on [21/07/2025]. See the Terms and Conditions (https://onlinelibrary.wiley.com/terms-and-conditions) on Wiley Online Library for rules of use; OA articles are governed by the applicable Creative Commons License

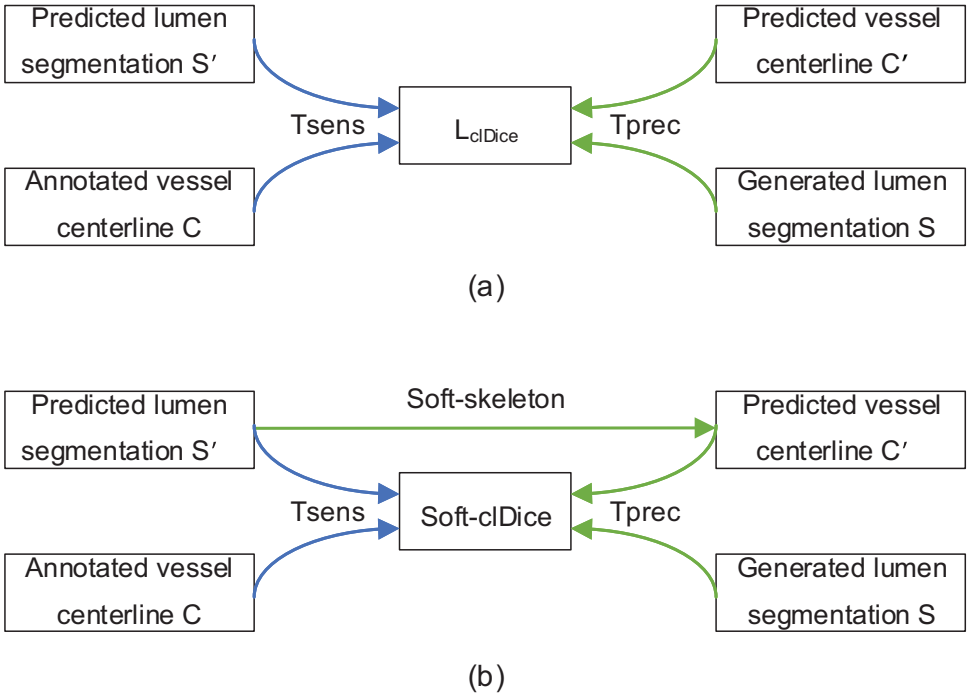

FIGURE 6 Comparison between (a) L_{clDice} and (b) the soft-clDice.

strategy to evaluate the proposed framework. In each fold, eight intracranial CTA images and 32 cube CTA images were used for training, while the remaining CTA images were used for testing.

3.2 | Evaluation metrics

We evaluated the proposed framework in terms of average symmetric centerline distance (ASCD) and overlap (OV) with reference to the experimental setup.[38,39] These are defined as follows:

ASCD: given target centerline points X and predicted centerline points Y, the average centerline distance (ACD) is computed as:

$$\mathrm{ACD}(X, Y) = \sum_{x \in X} min_{y \in Y} d(x, y)/|X| \tag{10}$$

where $d(x, y)$ is a 3D matrix consisting of the Euclidean distances between X and Y. And ASCD is formulated as:

$$\mathrm{ASCD}(X, Y) = \frac{\mathrm{ACD}(X, Y) + \mathrm{ACD}(Y, X)}{2} \tag{11}$$

OV: given target centerline points X and predicted centerline points Y, TP_T^R (true positives of the reference) are those points in X that have a point $y \in Y$ with a Euclidean distance less than a threshold T, and the other points in X are FN_T^R (false negatives of the reference). Similarly, TP_T^M (true positives of the model) are those points in Y that have a point $x \in X$ with a Euclidean distance less than a threshold T, and the other points in Y are FP_T^M (false positives of the model). In our experiments, we adopted two thresholds T (i.e., 1.0 and 1.5 mm) based on the average voxel spacing of $0.48 \times 0.48 \times 0.42$mm within the dataset. With these definitions, OV_T is defined as:

$$\mathrm{OV}_T = \frac{\mathrm{TP}_T^R + \mathrm{TP}_T^M}{\mathrm{TP}_T^R + \mathrm{TP}_T^M + \mathrm{FN}_T^R + \mathrm{FP}_T^M} \tag{12}$$

3.3 | Choosing optimization targets

Recently, a variety of optimization targets have been adopted for vessel centerline extraction from medical images, such as the distance map[17] and the heatmap.[19] In this paper, the proposed framework uses both the vessel centerline and the lumen segmentation as the optimization targets. While the proposed framework (and similar methods) defines a segmentation task, optimizing a distance map or a heatmap is a regression task.

In order to investigate the impact of different types of optimization targets, we constructed a distance map and a heatmap based on the distance to the centerline, as shown in Figures 7 and 8. Since the proposed framework had two optimization targets (i.e., centerline + lumen), a dual-branch 3D UNet (i.e., the DTUNet without the FP) was used to solve the two-target optimization problem. In contrast, a single 3D UNet was utilized for the remaining single optimization targets

24734209, 2025, 7, Downloaded from https://aapm.onlinelibrary.wiley.com/doi/10.1002/mp.17855, Wiley Online Library on [21/07/2025]. See the Terms and Conditions (https://onlinelibrary.wiley.com/terms-and-conditions) on Wiley Online Library for rules of use; OA articles are governed by the applicable Creative Commons License

TABLE 2 Comparison among various types of optimization targets by five-fold cross-validation analysis.

Target	Task type	Intracranial			Cube		
		ASCD (mm) ↓	$OV_{1.0}$ ↑	$OV_{1.5}$ ↑	ASCD (mm) ↓	$OV_{1.0}$ ↑	$OV_{1.5}$ ↑
Distance map	Regression	1.20 ± 0.11	0.708 ± 0.039	0.806 ± 0.024	1.78 ± 0.46	0.649±0.052	0.741±0.050
Heatmap	Regression	1.08±0.11	0.782±0.014	0.837±0.017	1.49±0.40	0.735±0.044	0.792±0.043
Centerline	Segmentation	1.05±0.07	0.794±0.014	0.840±0.012	1.66±0.37	0.722±0.037	0.769±0.037
Lumen	Segmentation	0.95±0.08	0.810±0.014	0.859±0.012	1.40±0.39	0.752±0.049	0.803±0.046
Centerline + Lumen	Segmentation	**0.89±0.06**†	**0.832±0.009**†	**0.880±0.009**†	**1.28±0.29**†	**0.773±0.042**†	**0.821±0.041**†

Note: † indicates statistically a significant difference of $p < 0.05$ between the centerline + lumen and the other optimization targets in a paired *t*-test.
Abbreviations: ASCD, average symmetric centerline distance; OV, overlap.

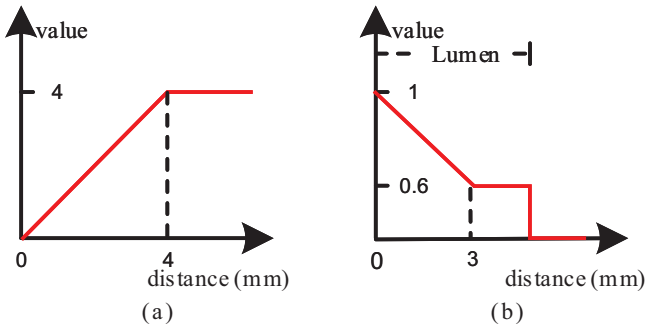

FIGURE 7 A schematic diagram of (a) the distance map and (b) the heatmap.

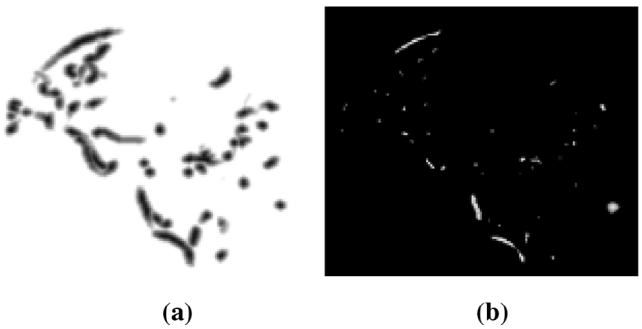

FIGURE 8 A typical example of (a) the distance map and (b) the heatmap, where red points denote vessel centerlines.

(i.e., the distance map, the heatmap, the centerline, and the lumen). In this way, we aim to minimize the influence of model architecture changes on the performance of centerline extraction, and thus more fairly assess the effectiveness of the optimization targets. Table 2 reports the centerline extraction results of the different types of optimization targets. Compared to the regression tasks, the lumen and the centerline + lumen both obtain better results. The centerline also obtains comparable results to the heatmap. Moreover, in the segmentation tasks, the lumen obtains superior results to the centerline. This suggests that the lumen is more suitable as an optimization target for vessel centerline extraction compared to the centreline. Lastly, combining both the centerline and the lumen achieves the best results, which significantly outperforms other optimization targets. Therefore, combining the centerline and the lumen is a well-suited optimization target for the vessel centerline extraction from CTA images.

3.4 | Hyper-parameter α of the TAL

We studied the effect of the hyper-parameter α of the TAL on the DTUNet. Figure 9 shows the results of the DTUNet with seven different values for α (i.e., 0, 0.1, 0.2, 0.3, 0.4, 0.5, and 0.6). $\alpha = 0$ means that DTUNet is optimized by L_{Dice}^{seg} and L_{Dice}^{cen}, while $\alpha > 0$ means that the DTUNet is optimized by L_{Dice}^{seg}, L_{Dice}^{cen} and L_{clDice}. Starting from a small α, an increase of α improves the performance of the DTUNet on ASCD, $OV_{1.0}$ and $OV_{1.5}$. The DTUNet achieves the best performance at $\alpha = 0.2$; the performance of the DTUNet decreases rapidly when $\alpha > 0.2$, and is even worse than the performance at $\alpha = 0$ in the end. Based on these experiments, we chose 0.2 as the value of the hyper-parameter α for DTUNet, in the following experiments unless otherwise specified.

3.5 | Ablation studies

We conducted an ablation study to evaluate the contributions of lumen segmentation, TAL, and various backbones on the performance of the DTUNet (Table 3). It should be noted that "use of lumen" denotes that networks are trained with both vessel centerline annotations and the generated lumen segmentation, while the term "no use of lumen" indicates that networks are trained exclusively using vessel centerline annotations. Similarly, the term "use of TAL" refers to training the network using the TAL function, whereas the term "no use of TAL" indicates that the training relies exclusively on the Dice loss function. Table 3 shows that compared to the 3D UNet that directly predicts the vessel centerline, the 3D UNet trained with the lumen segmentation achieves statistically significantly ($p < 0.05$) better results across all the metrics. This improvement suggests that the lumen segmentation helps the 3D UNet extract the vessel centerlines from CTA images. Table 3 also illustrates that the TAL provides substantial benefits

24734209, 2025, 7, Downloaded from https://aapm.onlinelibrary.wiley.com/doi/10.1002/mp.17855, Wiley Online Library on [21/07/2025]. See the Terms and Conditions (https://onlinelibrary.wiley.com/terms-and-conditions) on Wiley Online Library for rules of use; OA articles are governed by the applicable Creative Commons License

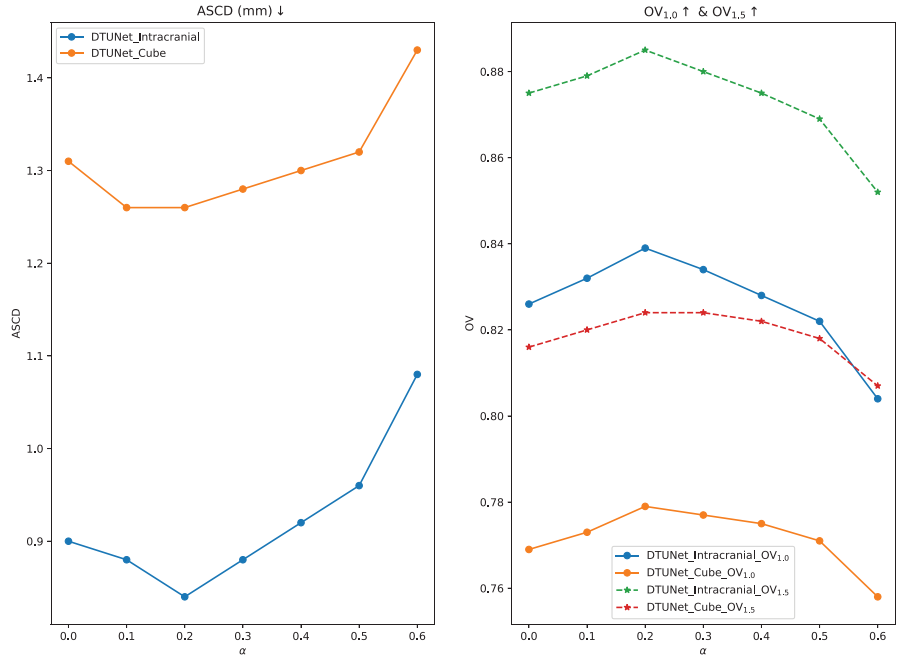

FIGURE 9 Five-fold cross-validation results of DTUNet with different hyper-parameters α. DTUNet, dual-branch topology-aware UNet.

TABLE 3 Ablation study.

Backbone	Lumen	TAL	Intracranial			Cube		
			ASCD (mm) ↓	$OV_{1.0}$ ↑	$OV_{1.5}$ ↑	ASCD (mm) ↓	$OV_{1.0}$ ↑	$OV_{1.5}$ ↑
3D UNet			1.05±0.07	0.794±0.014	0.840±0.012	1.66±0.37	0.722±0.037	0.769±0.037
3D UNet	√		0.95±0.08	0.810±0.014	0.859±0.012	1.40±0.39	0.752±0.049	0.803±0.046
DTUNet w/o FP	√		0.92±0.09	0.820±0.012	0.870±0.015	1.33±0.41	0.767±0.045	0.816±0.046
DTUNet w/o FP	√	√	0.89±0.06	0.832±0.009	0.880±0.009	1.28±0.29	0.773±0.042	0.821±0.041
DTUNet	√		0.90±0.08	0.826±0.008	0.875±0.009	1.31±0.32	0.769±0.043	0.816±0.041
DTUNet	√	√	**0.84±0.07**	**0.839±0.008**	**0.885±0.010**	**1.26±0.29**	**0.779±0.043**	**0.824±0.041**

Abbreviations: ASCD, average symmetric centerline distance; DTUNet, dual-branch topology-aware UNet; FP, fusion path; OV, overlap.

to DTUNets with and without the FP. This reveals that the TAL can further improve the performance of the models by optimizing the consistency of the topological connectivity between the predicted vessel centerline and the predicted lumen segmentation. In addition, the complete DTUNet architecture, which includes the FP, marginally outperforms the DTUNet variant without this component. Most notably, the DTUNet trained with the lumen segmentation significantly outperforms the 3D UNet that also incorporates lumen segmentation, across all the metrics ($p < 0.05$). These findings highlight the DTUNet's strong capability in processing complex vascular structures within CTA images.

3.6 | Comparison with a 3D UNet trained using the soft-clDice + soft-Dice

The method of Shit et al.[34] (i.e., the 3D UNet trained using the soft-clDice + soft-Dice) also utilizes the clDice loss fucntion and Dice loss function for network optimization. However, the proposed framework exploits an elaborate two-branch architecture and a distinct loss computation process, as detailed in Section 2.3. Therefore, we compared the proposed framework with the the 3D UNet trained using the soft-clDice + soft-Dice. It is worth noting that in the latter method, we also used the medial surface/axis thinning algorithm[35] to obtain the final vessel centerlines from the predicted lumen segmentation since its soft-skeleton algorithm is designed for gradient backpropagation purposes rather than for smoothing the vessel centerlines. Table 4 reports the results of the DTUNet and the 3D UNet trained using the soft-clDice + soft-Dice. The result of the DTUNet is superior to the result of the 3D UNet trained using the soft-clDice + soft-Dice. This finding validates the superior capability of the dual-branch architecture and the proposed TAL in extracting vessel centerlines from CTA images. Moreover, the segmentation branch of the DTUNet achieves better performance

24734209, 2025, 7, Downloaded from https://aapm.onlinelibrary.wiley.com/doi/10.1002/mp.17855, Wiley Online Library on [21/07/2025]. See the Terms and Conditions (https://onlinelibrary.wiley.com/terms-and-conditions) on Wiley Online Library for rules of use; OA articles are governed by the applicable Creative Commons License

TABLE 4 Comparison between the DTUNet (without the FP) trained using the TAL and the 3D UNet of Shit et al. by five-fold cross-validation analysis.

Method	Output	Intracranial			Cube		
		ASCD (mm) ↓	$OV_{1.0}$ ↑	$OV_{1.5}$ ↑	ASCD (mm) ↓	$OV_{1.0}$ ↑	$OV_{1.5}$ ↑
3D UNet[34]	Lumen + thining[35]	0.90±0.07	0.825±0.008	0.871±0.006	1.34±0.35	0.770±0.043	0.815±0.042
DTUNet	Centerline	0.89±0.05	0.830±0.006	0.878±0.008	1.31±0.36	0.773±0.042	0.819±0.041
DTUNet	Lumen + thining[35]	**0.84±0.07**†	**0.839±0.008**†	**0.885±0.010**†	**1.26±0.29**†	**0.779±0.043**†	**0.824±0.041**†

Note: † indicates a statistically significant difference of $p < 0.05$ in a paired *t*-test compared to other methods.
Abbreviations: ASCD, average symmetric centerline distance; DTUNet, dual-branch topology-aware UNet; FP, fusion path; OV, overlap; TAL, topology-aware loss.

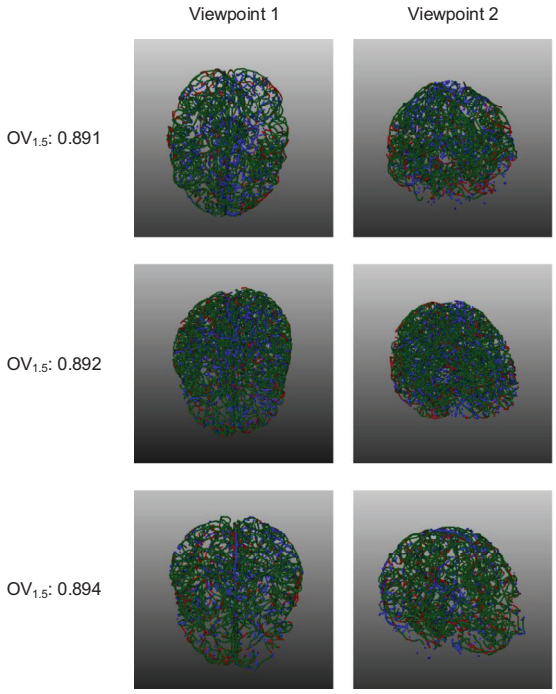

FIGURE 10 Visualization of three example intracranial cases with two different viewpoints. Green points are true positives; blue points are false positives; red points are false negatives. In addition, values of the $OV_{1.5}$ metric are indicated for all the cases. OV, overlap.

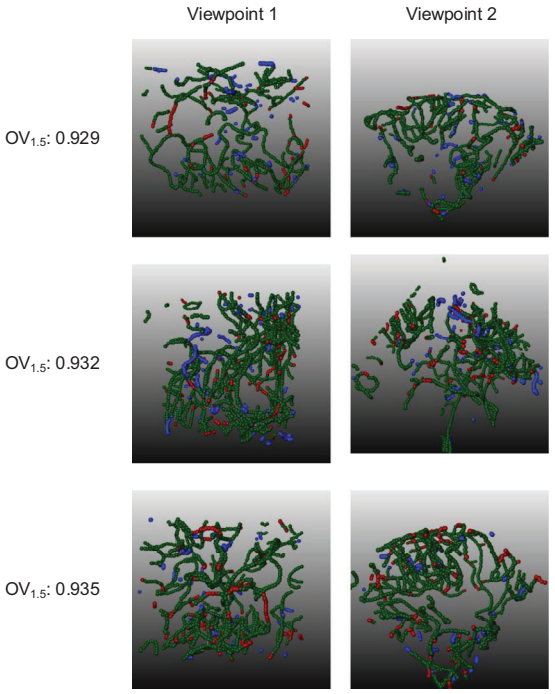

FIGURE 11 Visualization of three example cube cases with two different viewpoints. Green points are true positives; blue points are false positives; red points are false negatives. In addition, values of the $OV_{1.5}$ metric are indicated for all the cases. OV, overlap.

than the centerline branch, with statistically significant improvements. These results indicate that extracting the final vessel centerlines from the lumen segmentation output by the segmentation branch represents a more effective choice.

3.7 | Subgroup analyses

We further computed the performance of the proposed framework on various subgroups, based on vessel radius and location. To this end, we computed the vessel radius per segment by averaging the radii of the lumen segmentation generated by the lumen segmentation generation algorithm. Based on the histogram of the vessel radius (Figure 12), the vessel segments were grouped into three categories: thin vessels (radius ≤ 0.6mm), medium vessels (0.6mm < radius ≤ 1.0mm), and large vessels (radius > 1.0mm). It should be noted that the average radius of the vessels tends to be smaller than those reported in medical studies.[40–42] This discrepancy may be attributed to the under-segmented nature of the lumen segmentation generation algorithm as well as the multiple averaging operations used to calculate the vessel radius. To group the vessel segments based on location, we applied the same registration approach mentioned in pre-processing to obtain a hemisphere mask, a middle cerebral artery (MCA) mask, an anterior cerebral artery (ACA) mask, and a posterior cerebral artery (PCA) mask, according to the work of ref. [43]. The vessel segments were subsequently assigned to one of these regions. Since the proposed framework did not output the vessel radius, we could not obtain the vessel thickness types of the predicted centerlines. Therefore, ASCD and OV could no longer be computed, and instead we used the average centerline distance (ACD) that only computed the Euclidean distances from the target centerline points

24734209, 2025, 7, Downloaded from https://aapm.onlinelibrary.wiley.com/doi/10.1002/mp.17855, Wiley Online Library on [21/07/2025]. See the Terms and Conditions (https://onlinelibrary.wiley.com/terms-and-conditions) on Wiley Online Library for rules of use; OA articles are governed by the applicable Creative Commons License

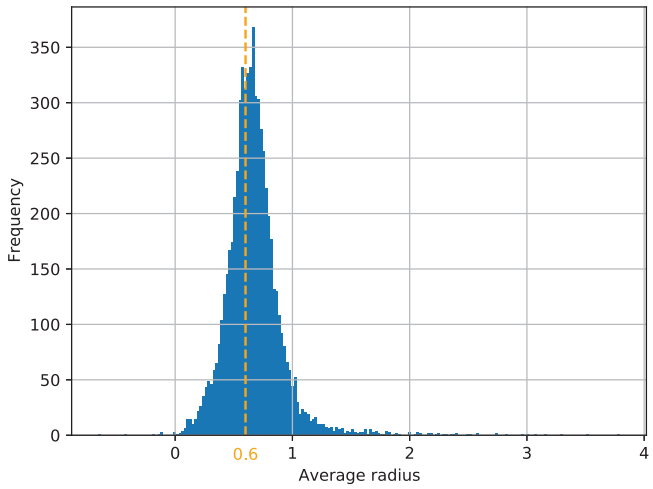

FIGURE 12 Histogram of the average radius of the vessels for 10 intracranial CTA images. The position corresponding to an average radius of 0.6 is indicated with an orange dashed line. The average radius of the vessels tends to be smaller than those reported in medical studies due to the under-segmentation as well as the multiple averaging operations. CTA, computed tomographic angiography.

TABLE 5 Subgroup analyses of the proposed framework.

Property	Category	ACD (mm) ↓	$Recall_{1.0}$ ↑	$Recall_{1.5}$ ↑
Vessel thickness	Thin	0.87±0.11	0.798±0.011	0.861±0.016
	Medium	0.63±0.09	0.875±0.017	0.920±0.019
	Large	0.85±0.10	0.753±0.035	0.873±0.023
Region	Left hemisphere	0.72±0.08	0.847±0.016	0.901±0.017
	Right hemisphere	0.70±0.06	0.859±0.017	0.910±0.018
	MCA region	0.47±0.06	0.931±0.015	0.963±0.017
	ACA region	0.49±0.06	0.918±0.025	0.958±0.019
	PCA region	0.41±0.07	0.949±0.031	0.983±0.018

Abbreviations: ACD, average centerline distance; ACA, anterior cerebral artery; MCA, middle cerebral artery; PCA, posterior cerebral artery.

to the predicted centerline points, and the recall as the evaluation metrics.

Table 5 presents the subgroup analyses of the proposed framework. It is evident from this table that the proposed framework achieves better results for medium vessels than for thin and large vessels. We observe no significant difference in the results between the left and right hemispheres, despite the fact that these brains suffered from acute ischemic stroke. The proposed framework also demonstrates encouraging results for the MCA region, the ACA region, and the PCA region.

3.8 | Comparison with state-of-the-art methods

In this experiment, we quantitatively compared the proposed framework with the state-of-the-art methods widely used for vessel segmentation and vessel centerline extraction, including 3D UNet,[33] VNet,[44] Su's net,[6] CS^2Net,[45] TransBTS,[46] and UNETR.[47] From Table 6, it is evident that the proposed framework achieves better performance than the state-of-the-art methods across all the metrics, with statistically significant improvements.

We also qualitatively analysed the proposed framework and compared it with 3D UNet and TransBTS. Figures 10 and 11 visualize the results of the proposed framework for an intracranial case and a cube case, respectively. The proposed framework correctly predicts most of the vessel centerlines, with only a few false positives and false negatives. Figure 13 visualizes the results of the proposed framework, 3D UNet, and TransBTS for an intracranial case and a cube case, respectively. Compared with the 3D UNet and TransBTS, the proposed framework predicts more vessel centerlines correctly, at the expense of a few more false positives.

4 | DISCUSSION

In this paper, we presented and assessed a segmentation-assisted framework for brain vessel centerline extraction from CTA images. Comprehensive experiments on an in-house dataset demonstrated the effectiveness of each of its components and its superiority over the state-of-the-art methods.

The proposed framework has demonstrated promising results across various vessel sizes, although it exhibits superior performance on medium vessels relative to both finer and larger ones (Table 5). This variation in performance can be attributed to the inherent challenges associated with each vessel type. Specifically, the centerlines of thin vessels are often missed due to their subtle nature. The centerlines of large vessels are more difficult to predict due to two primary factors. First, the labeling of their centerlines is inherently not well-centered. Secondly, the generated lumen segmentation, which serves as supervisory information, is somewhat less accurate due to the increased size of the lumen. Additionally, our analysis reveals no significant difference in the results between the left and right hemispheres in stroke patients. This suggests that the proposed framework may be applied to the collateral circulation assessment in stroke patients. For example, the automated collateral method proposed by Su et al.[6] required a comparison of vascular features between an affected hemisphere and a non-affected hemisphere. Moreover, the framework shows encouraging centerline extraction performance in each of the MCA, ACA, and PCA regions. Such regions play a vital role in the treatment of stroke, such as arterial thrombolysis. These findings indicate that the proposed framework holds the potential for quantitative analysis of the brain vasculature. This could be highly relevant for stroke research and treatment decision-making.[2]

24734209, 2025, 7, Downloaded from https://aapm.onlinelibrary.wiley.com/doi/10.1002/mp.17855, Wiley Online Library on [21/07/2025]. See the Terms and Conditions (https://onlinelibrary.wiley.com/terms-and-conditions) on Wiley Online Library for rules of use; OA articles are governed by the applicable Creative Commons License

TABLE 6 Comparison with the state-of-the-art methods.

Method	Intracranial			Cube		
	ASCD (mm) ↓	$OV_{1.0}$ ↑	$OV_{1.5}$ ↑	ASCD (mm) ↓	$OV_{1.0}$ ↑	$OV_{1.5}$ ↑
3D UNet[33]	1.05±0.07	0.794±0.014	0.840±0.012	1.66±0.37	0.722±0.037	0.769±0.037
VNet[44]	1.18±0.12	0.769±0.021	0.820±0.019	1.68±0.42	0.703±0.039	0.756±0.039
Su's net[6]	1.01±0.07	0.802±0.006	0.849±0.007	1.48±0.34	0.739±0.044	0.789±0.044
CS^2Net[45]	1.05±0.10	0.792±0.012	0.839±0.012	1.59±0.37	0.720±0.036	0.768±0.038
TransBTS[46]	0.98±0.10	0.811±0.011	0.856±0.017	1.42±0.26	0.744±0.035	0.793±0.034
UNETR[47]	1.18±0.08	0.750±0.010	0.808±0.008	1.58±0.32	0.694±0.043	0.757±0.043
Proposed	**0.84±0.07**⋆	**0.839±0.008**⋆	**0.885±0.010**⋆	**1.26±0.29**†	**0.779±0.043**†	**0.824±0.041**†

Note: ⋆ and † indicate a statistically significant difference of $p < 0.01$ and $p < 0.05$ between the proposed framework and the state-of-the-art methods in a paired *t*-test, respectively.
Abbreviations: ASCD, average symmetric centerline distance; DTUNet, dual-branch topology-aware UNet; OV, overlap.

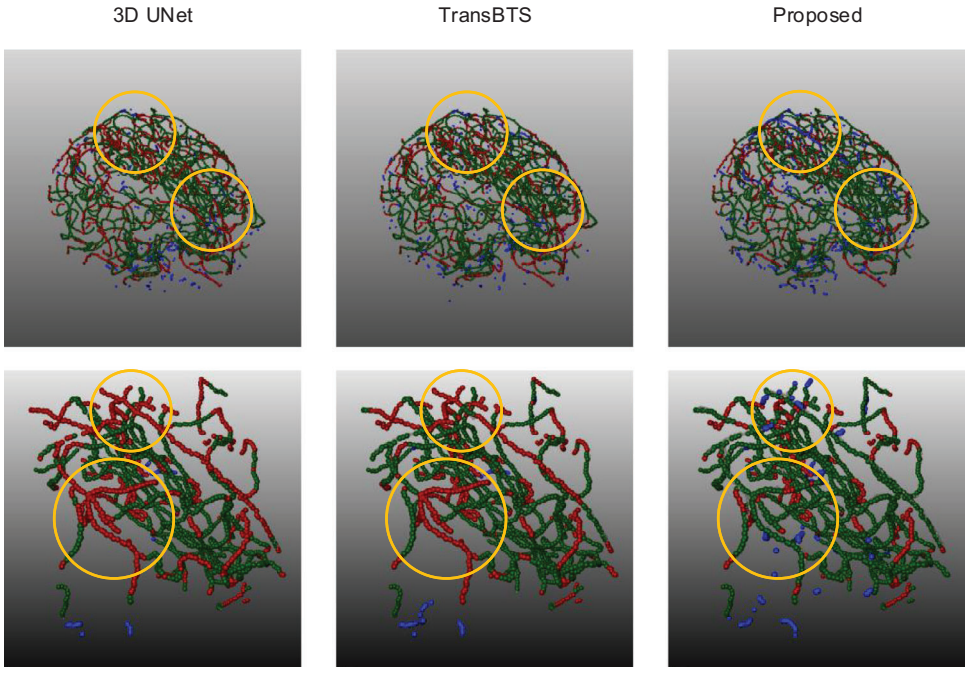

FIGURE 13 Visualization of the results of different methods for an intracranial case and a cube case. The first row and the second row show the results of the intracranial case and the cube case, respectively. Green points are true positives; blue points are false positives; red points are false negatives. Yellow circles highlight the areas where the results differ.

The proposed framework exploits the lumen segmentation generation algorithm based on centerlines, originally introduced by M. Schaap et al.,[29] to provide additional supervisory information for training deep neural networks. This effectively alleviates the reliance on labor-intensive manual lumen annotation efforts, addressing the scalability limitations of current neural network-based methods. The ablation study in Table 3 has demonstrated that incorporating this algorithm substantially improves vessel centerline extraction performance. While initially designed for coronary lumen segmentation, the algorithm has exhibited high segmentation accuracy in cerebral vessel centerline extraction. This consistency in performance across different vascular structures suggests its potential for broader application in the lumen segmentation of various other 3D vasculatures.

The proposed framework also demonstrates good performance of the centerline branch in extracting vessel centerlines from CTA images. As shown in Tables 3 and 4, the centerline branch of the proposed DTUNet outperforms both the 3D UNet that directly predicts vessel centerlines and the 3D UNet trained using lumen segmentation supervision. This highlights that the dual-branch architecture, along with the proposed TAL, not only enhances the lumen segmentation branch but also optimizes the direct prediction of vessel centerlines.

24734209, 2025, 7, Downloaded from https://aapm.onlinelibrary.wiley.com/doi/10.1002/mp.17855, Wiley Online Library on [21/07/2025]. See the Terms and Conditions (https://onlinelibrary.wiley.com/terms-and-conditions) on Wiley Online Library for rules of use; OA articles are governed by the applicable Creative Commons License

While the proposed framework shows promising performance in brain vessel centerline extraction from CTA images, areas of improvement remain. In the regions near the skull, vessels tend to be thinner and less distinct, often blending in with the surrounding tissues due to similar intensity levels. The current framework may overlook such vessels as it lacks specific mechanisms to handle these low-contrast scenarios. Future work could involve the development of methods designed to enhance the detection and segmentation of thin, low-contrast vessels. Additionally, we have noted instances where vessel centerline segments predicted by the framework are not fully connected, despite belonging to the same continuous vessel. This fragmentation can complicate the tracking and comprehensive analysis of the vascular network. To mitigate this issue, further research into post-processing techniques aimed at connecting disjointed centerline segments could be beneficial. Moreover, several studies have shown that overlapping patch fusion can enhance edge segmentation accuracy, leading to improved overall segmentation performance. In the proposed framework, the final vessel centerlines are derived from thinning the lumen segmentation. Consequently, the overlapping patch fusion algorithm may offer further improvements. One more thing; although the vessel lumen derived from the lumen segmentation generation algorithm was verified by an expert with decades of experience in vascular research, its accuracy is still insufficient in certain scenarios, particularly with kissing vessels. Despite the robust feature extraction capabilities of deep neural networks, the use of inaccurate vascular lumens as supervisory information can adversely affect network training to some extent. Future research could focus on the development of an enhanced centerline-based lumen segmentation generation algorithm.

5 | CONCLUSION

In this study, we have developed and validated a segmentation-assisted framework for brain vessel centerline extraction from CTA images. The proposed solution leverages lumen segmentation generated from annotated centerlines during the training phase, which we have shown to significantly enhance centerline extraction performance without necessitating additional annotation efforts. We show that the dual-branch DTUNet, supported by a TAL function, effectively utilizes both annotated vessel centerlines and the generated lumen segmentation during training. Extensive experiments on an in-house dataset demonstrate its superiority over state-of-the-art methods on the ASCD and OV metrics. Subgroup analyses further highlight its potential in clinical applications for cerebrovascular disease diagnosis and treatment.

ACKNOWLEDGMENTS

This work was supported in part by the National Key Research and Development Program of China under grant 2017YFA0700800. This work was also supported by Health-Holland (TKI Life Sciences and Health) through the Q-Maestro project under Grant EMCLSH19006 and Philips Healthcare (Best, The Netherlands). We acknowledge the support of the Netherlands Cardiovascular Research Initiative which is supported by the Dutch Heart Foundation (CVON2015-01: CONTRAST), the support of the Brain Foundation Netherlands (HA2015.01.06), and the support of Health-Holland, Top Sector Life Sciences & Health (LSHM17016), Medtronic, Cerenovus and Stryker European Operations BV. The collaboration project is additionally financed by the Ministry of Economic Affairs by means of the PPP Allowance made available by the Top Sector Life Sciences & Health to stimulate public-private partnerships.

CONFLICT OF INTEREST STATEMENT

The authors declare no conflicts of interest.

DATA AVAILABILITY STATEMENT

Code has been made available at https://github.com/Liusj-gh/DTUNet.

REFERENCES

1. WHO EMRO | Stroke, Cerebrovascular accident | Health topics — emro.who.int. Accessed 29-04-2024. https://www.emro.who.int/health-topics/stroke-cerebrovascular-accident/index.html
2. Peisker T, Koznar B, Stetkarova I, Widimsky P. Acute stroke therapy: a review. *Trends Cardiovasc Med*. 2017;27:59-66.
3. El-Baz A, Elnakib A, Khalifa F, et al. Precise segmentation of 3-D magnetic resonance angiography. *IEEE Trans Biomed Eng*. 2012;59:2019-2029.
4. Soltanpour M, Greiner R, Boulanger P, Buck B. Improvement of automatic ischemic stroke lesion segmentation in CT perfusion maps using a learned deep neural network. *Comput Biol Med*. 2021;137:104849.
5. Stib MT, Vasquez J, Dong MP, et al. Detecting large vessel occlusion at multiphase CT angiography by using a deep convolutional neural network. *Radiology*. 2020;297:640-649.
6. Su J, Wolff L, van Es ACM, et al. Automatic collateral scoring from 3D CTA images. *IEEE Trans Med Imaging*. 2020;39:2190-2200.
7. Lv T, Yang G, Zhang Y, et al. Vessel segmentation using centerline constrained level set method. *Multimed Tools Appl*. 2019;78:17051-17075.
8. Reinertsen I, Lindseth F, Unsgaard G, Collins DL. Clinical validation of vessel-based registration for correction of brain-shift. *Med Image Anal*. 2007;11:673-684.
9. Palágyi K, Balogh E, Kuba A, et al. A sequential 3D thinning algorithm and its medical applications. In: *Information Processing in Medical Imaging: 17th International Conference, IPMI 2001 Davis, CA, USA, June 18–22, 2001*. Springer; 2001:409-415.
10. Cheng Y, Hu X, Wang Y, Wang J, Tamura S. Automatic centerline detection of small three-dimensional vessel structures. *J Electron Imaging*. 2014;23:013007-013007.
11. He T, Hong L, Chen D, Liang Z. Reliable path for virtual endoscopy: Ensuring complete examination of human organs. *IEEE Trans Vis Comput Graph*. 2001;7:333-342.

24734209, 2025, 7, Downloaded from https://aapm.onlinelibrary.wiley.com/doi/10.1002/mp.17855, Wiley Online Library on [21/07/2025]. See the Terms and Conditions (https://onlinelibrary.wiley.com/terms-and-conditions) on Wiley Online Library for rules of use; OA articles are governed by the applicable Creative Commons License

12. Jin D, Iyer KS, Chen C, Hoffman EA, Saha PK. A robust and efficient curve skeletonization algorithm for tree-like objects using minimum cost paths. *Pattern Recognit Lett*. 2016;76:32-40.
13. Krissian K, Malandain G, Ayache N, Vaillant R, Trousset Y. Model-based detection of tubular structures in 3D images. *Comput Vis Image Underst*. 2000;80:130-171.
14. Fung EK, Carson RE. Cerebral blood flow with [15O] water PET studies using an image-derived input function and MR-defined carotid centerlines. *Phys Med Biol*. 2013;58:1903.
15. Moccia S, De Momi E, El Hadji S, Mattos LS. Blood vessel segmentation algorithms–review of methods, datasets and evaluation metrics. *Comput Methods Programs Biomed*. 2018;158:71-91.
16. Xiao H, Li L, Liu Q, Zhu X, Zhang Q. Transformers in medical image segmentation: a review. *Biomed Signal Process Control*. 2023;84:104791.
17. Guo Z, Bai J, Lu Y, et al. Deepcenterline: A multi-task fully convolutional network for centerline extraction. In: *Information Processing in Medical Imaging: 26th International Conference, IPMI 2019, Hong Kong, China, June 2–7, 2019*. Springer; 2019:441-453.
18. Tetteh G, Efremov V, Forkert ND, et al. Deepvesselnet: Vessel segmentation, centerline prediction, and bifurcation detection in 3-d angiographic volumes. *Front Neurosci*. 2020;14:592352.
19. He J, Pan C, Yang C, et al. Learning hybrid representations for automatic 3D vessel centerline extraction. In: *Medical Image Computing and Computer Assisted Intervention–MICCAI 2020: 23rd International Conference, Lima, Peru, October 4–8, 2020*. Springer; 2020:24-34.
20. Sironi A, Türetken E, Lepetit V, Fua P. Multiscale centerline detection. *IEEE Trans Pattern Anal Mach Intell*. 2015;38:1327-1341.
21. Rjiba S, Urruty T, Bourdon P, et al. CenterlineNet: automatic coronary artery centerline extraction for computed tomographic angiographic images using convolutional neural network architectures. In: *2020 Tenth International Conference on Image Processing Theory, Tools and Applications (IPTA)*. IEEE; 2020:1-6.
22. Zhang X, Du H, Song G, et al. X-ray coronary centerline extraction based on C-UNet and a multifactor reconnection algorithm. *Comput Methods Programs Biomed*. 2022;226:107114.
23. Zhang P, Wang F, Zheng Y. Deep reinforcement learning for vessel centerline tracing in multi-modality 3D volumes. In: *Medical Image Computing and Computer Assisted Intervention–MICCAI 2018: 21st International Conference, Granada, Spain, September 16-20, 2018*. Springer; 2018:755-763.
24. Wolterink JM, van Hamersvelt RW, Viergever MA, Leiner T, Išgum I. Coronary artery centerline extraction in cardiac CT angiography using a CNN-based orientation classifier. *Med Image Anal*. 2019;51:46-60.
25. Jansen IG, Mulder MJ, Goldhoorn R-JB. Endovascular treatment for acute ischaemic stroke in routine clinical practice: prospective, observational cohort study (MR CLEAN Registry). *BMJ*. 2018;360:k949.
26. Heckel F, Schwier M, Peitgen H-O. Object-oriented application development with MeVisLab and Python. 2009.
27. Friston KJ. Statistical parametric mapping. In: *Neuroscience databases: a practical guide*. Elsevier; 2003:237-250.
28. Avants BB, et al. Advanced normalization tools (ANTS). *Insight J*. 2009;2:1-35.
29. Schaap M, Neefjes L, Metz C, et al. Coronary lumen segmentation using graph cuts and robust kernel regression. In: *International Conference on Information Processing in Medical Imaging*. Springer; 2009:528-539.
30. Boykov Y, Veksler O, Zabih R. Markov random fields with efficient approximations. In: *Proceedings. 1998 IEEE Computer Society Conference on Computer Vision and Pattern Recognition (Cat. No. 98CB36231)*. IEEE; 1998:648-655.
31. Debruyne M, Hubert M, Suykens JA. c. *Journal of Machine Learning Research-Cambridge, Mass*. 2008;9:2377-2400.
32. Heckel F, Konrad O, Hahn HK, Peitgen H-O. Interactive 3D medical image segmentation with energy-minimizing implicit functions. *Comput Graphics*. 2011;35:275-287.
33. Çiçek Ö, Abdulkadir A, Lienkamp SS, Brox T, Ronneberger O. 3D U-Net: learning dense volumetric segmentation from sparse annotation. In: *Medical Image Computing and Computer-Assisted Intervention–MICCAI 2016: 19th International Conference, Athens, Greece, October 17-21, 2016*. Springer; 2016:424-432.
34. Shit S, Paetzold JC, Sekuboyina A, et al. clDice-a novel topology-preserving loss function for tubular structure segmentation. In: *Proceedings of the IEEE/CVF conference on computer vision and pattern recognition*, 2021:16560-16569.
35. Lee T-C, Kashyap RL, Chu C-N. Building skeleton models via 3-D medial surface axis thinning algorithms. *CVGIP: Graphical Models and Image Processing*. 1994;56:462-478.
36. Paszke A, Gross S, Massa F, et al. Pytorch: An imperative style, high-performance deep learning library. *Adv Neural Inf Process Syst*. 2019;32:8026-8037.
37. Kingma DP, Ba J. Adam: A method for stochastic optimization. *arXiv preprint arXiv:1412.6980* 2014.
38. Tang S, Chan CS. Orthogonal planar search (OPS) for coronary artery centerline extraction. *Signal Image Video Process*. 2016;10:335-342.
39. Zhu C, Wang X, Chen S, Xia M, Huang Y, Pan X. Automatic centerline extraction of cerebrovascular in 4D CTA based on tubular features. *Phys Med Biol*. 2018;63:125014.
40. Pai S, Kulkarni R, Varma R. Microsurgical anatomy of the anterior cerebral artery-anterior communicating artery complex: an indian study. *Neurology Asia*. 2005;10:21-28.
41. Pai SB, Varma R, Kulkarni R. Microsurgical anatomy of the middle cerebral artery. *Neurol India*. 2005;53:186-190.
42. Krishnamurthy A, Nayak S, Kumar CG, et al. Morphometry of posterior cerebral artery: embryological and clinical significance. *Rom J Morphol Embryol*. 2008;49:43-45.
43. Peter R, Emmer BJ, Van Es AC, Van Walsum T. Cortical and vascular probability maps for analysis of human brain in computed tomography images. In: *2017 IEEE 14th International Symposium on Biomedical Imaging (ISBI 2017)*. IEEE; 2017:1141-1145.
44. Milletari F, Navab N, Ahmadi S-A. V-net: Fully convolutional neural networks for volumetric medical image segmentation. In: *2016 fourth international conference on 3D vision (3DV)*. IEEE; 2016:565-571.
45. Mou L, Zhao Y, Fu H, et al. CS2-Net: deep learning segmentation of curvilinear structures in medical imaging. *Med Image Anal*. 2021;67:101874.
46. Wenxuan W, Chen C, Meng D, Hong Y, Sen Z, Jiangyun L. Transbts: multimodal brain tumor segmentation using transformer. In: *International Conference on Medical Image Computing and Computer-Assisted Intervention*. Springer; 2021:109-119.
47. Hatamizadeh A, Tang Y, Nath V, et al. Unetr: transformers for 3D medical image segmentation. In: *Proceedings of the IEEE/CVF winter conference on applications of computer vision*. IEEE; 2022:574-584.

How to cite this article: Liu S, Su R, Su J, et al. Segmentation-assisted vessel centerline extraction from cerebral CT Angiography. *Med Phys*. 2025;52:e17855.
https://doi.org/10.1002/mp.17855

24734209, 2025, 7, Downloaded from https://aapm.onlinelibrary.wiley.com/doi/10.1002/mp.17855, Wiley Online Library on [21/07/2025]. See the Terms and Conditions (https://onlinelibrary.wiley.com/terms-and-conditions) on Wiley Online Library for rules of use; OA articles are governed by the applicable Creative Commons License